NANO LETTERS

2008
Vol. 8, No. 3
891-896

Toward Atomic-Scale Bright-Field Electron Tomography for the Study of Fullerene-Like Nanostructures

Maya Bar Sadan,[†] Lothar Houben,[*,‡] Sharon G. Wolf,[§] Andrey Enyashin,[||] Gotthard Seifert,[||] Reshef Tenne,[†] and Knut Urban[‡]

Materials and Interfaces Department, Weizmann Institute of Science, Rehovot 76100, Israel, Institute of Solid State Research and Ernst-Ruska Centre for Microscopy and Spectroscopy with Electrons, Research Centre Jülich GmbH, 52425 Jülich, Germany, Electron Microscopy Unit, Weizmann Institute of Science, Rehovot 76100, Israel, and Physikalische Chemie, Technische Universität Dresden, 01062 Dresden, Germany

Received December 3, 2007; Revised Manuscript Received January 16, 2008

ABSTRACT

We present the advancement of electron tomography for three-dimensional structure reconstruction of fullerene-like particles toward atomic-scale resolution. The three-dimensional reconstruction of nested molybdenum disulfide nanooctahedra is achieved by the combination of low voltage operation of the electron microscope with aberration-corrected phase contrast imaging. The method enables the study of defects and irregularities in the three-dimensional structure of individual fullerene-like particles on the scale of 2–3 Å. Control over shape, size, and atomic architecture is a key issue in synthesis and design of functional nanoparticles. Transmission electron microscopy (TEM) is the primary technique to characterize materials down to the atomic level, albeit the images are two-dimensional projections of the studied objects. Recent advancements in aberration-corrected TEM have demonstrated single atom sensitivity for light elements at subångström resolution. Yet, the resolution of tomographic schemes for three-dimensional structure reconstruction has not surpassed 1 nm^3, preventing it from becoming a powerful tool for characterization in the physical sciences on the atomic scale. Here we demonstrate that negative spherical aberration imaging at low acceleration voltage enables tomography down to the atomic scale at reduced radiation damage. First experimental data on the three-dimensional reconstruction of nested molybdenum disulfide nanooctahedra is presented. The method is applicable to the analysis of the atomic architecture of a wide range of nanostructures where strong electron channeling is absent, in particular to carbon fullerenes and inorganic fullerenes.

Tomographic structure reconstruction is a well-established technique in transmission electron microscopy (TEM) in the field of biological sciences.[1–5] In contrast, there has been reluctance to use electron tomography in TEM as a basic tool for the analysis of solid-state structures in the physical sciences. Valuable shape and size information with a resolution of about 1 nm^3 is attained through recent progress in high-angle annular dark-field and energy-filtered tomography.[6–8] However, crucial information on molecular architecture or atomic coordination in a tomogram of individual nanoparticles demands even higher resolution on the scale of about 2 Å. Knowledge of the three-dimensional structure and composition on the atomic scale holds the key to understanding the unique physical properties of nanomaterials compared with their bulk counterparts. It is therefore one of the primary goals of electron tomography in material science to improve the resolution.

While bright-field high-resolution TEM offers the desired resolution, there are hitherto two main obstacles for atomic resolution bright-field tomography. First a resolution of around 2 Å could so far be achieved only at higher acceleration voltages, where severe radiation damage inhibits the recording of a sufficient number of tilt images of a single object. Second, bright-field images of crystalline material are subject to nonlinear dynamical diffraction and interference of the diffracted electron upon image recording. This implies that the "projection requirement", i.e., the requirement of the recorded signal to be related to a physical property in a monotonous manner, is usually not fulfilled.

Here we propose the application of low-voltage aberration-corrected bright-field electron tomography to overcome these obstacles to obtain three-dimensional (3D) reconstructions with atomic resolution of architectures without translatory periodicity and strong electron channelling effects. Therefore this technique is particularly applicable to fullerene structures, e.g., of inorganic layered compounds.[9–11] Here we will focus

* Corresponding author: l.houben@fz-juelich.de.
[†] Materials and Interfaces Department, Weizmann Institute of Science.
[‡] Institute of Solid State Research and Ernst-Ruska Centre for Microscopy and Spectroscopy with Electrons, Research Centre Jülich GmbH.
[§] Electron Microscopy Unit, Weizmann Institute of Science.
[||] Physikalische Chemie, Technische Universität Dresden.

10.1021/nl073149i CCC: $40.75
Published on Web 02/01/2008

on the closed-cage structures of inorganic fullerene-like nanoparticles.[9,10] An important morphology among these is the MoS_2 nanooctahedron, which is believed to be the smallest closed-cage structure of MoS_2 that is stable, i.e., the genuine inorganic fullerene. In previous studies, density functional tight-binding calculations proceeded by molecular dynamics annealing were used to elucidate the structure and electronic properties of octahedral MoS_2 fullerenes.[12,13] In contrast to bulk and nanotubular MoS_2, which are semiconductors, the Fermi level of the nanooctahedra is situated within Mo d-bands, rendering the nanoparticles metallic-like character. Since the electronic properties on the nanoscale are determined by the 3D construction of these atomic structures,[12,13] the ultimate goal of microscopy should be to decipher it. However, given the complexity of a nanoparticle such as the MoS_2 octahedron, simple high-resolution TEM imaging cannot resolve the true structure of the corners and edges. The convolved single projections can be only deciphered by tomography at atomic-scale resolution for a single particle, which is not available so far.

The basis for our approach to atomic-resolution tomography comprises new imaging modes for delocalization-reduced phase contrast in an aberration-corrected TEM[15–17] in combination with low-voltage operation, 80 kV in the present study. Both ingredients are essential for the atomic scale 3D reconstruction of the fullerene structures. The aberration correction assures that the point resolution of the microscope can extend to its information limit with insignificant residual point spread of the image detail.[14,15] Moreover, the setting of negative spherical aberration imaging (NCSI) yields images which are a close representation of the projected potential for weakly scattering objects and shows a high sensitivity even for light elements such as oxygen.[16,17] The point resolution of of about 2 Å at 80 kV in the NCSI mode outperforms the point resolution of conventional microscopes at much higher acceleration voltages while the rate for knock-on radiation damage is significantly reduced. Therefore, the NCSI mode at low acceleration voltage allows for the acquisition of a sufficient number of tilted object images with even superior resolution for the reconstruction for a wide range of materials where knock-on radiation damage is the primary source of damage.

In the following, a simulation study will provide evidence for the feasibility of atomic-resolution electron tomography based on aberration-corrected imaging and the first experimental data on the 3D reconstruction of the internal structure of a nested-shell MoS_2 nanooctahedron are presented.

For the simulation study, stoichiometric structure models of MoS_2 nanooctahedra calculated by the quantum mechanical approach in refs 12 and 13 were taken as reference models. Simulated tilt image series of nanoparticles were calculated from supercell data containing the atomic coordinates of the reference structures. For each viewing angle, the supercell coordinates were transformed accordingly. The supercells of a size of about $10 \times 10 \times 10$ nm^3 were divided into stacks of 3 Å thick slices for the multislice calculation of the electron wave propagation within the sample. The multislice iteration and the electron optical imaging were simulated using the EMS image calculation software.[19] NCSI conditions[17] were applied. At 80 kV accleration voltage, these are achieved at a negative spherical aberration of -52 μm that is balanced by an overfocus of $+17$ nm. NCSI imaging assures uniform contrast transfer up to the information limit of 0.2 nm, synonymous with a point resolution that matches the information limit. The residual point spread amounts to 0.11 nm, thus remaining smaller than the information limit. The tomographic reconstruction was carried out using the weighted backprojection algorithm implemented in the IMOD tomography software package.[20–22] AMIRA was used for isosurface visualization.[23]

MoS_2 nanooctahedra were prepared by laser ablation for the experiment. The details of the synthesis of MoS_2 nanooctahedra are presented elsewhere.[12] MoS_2 powder was pressed into a target pellet. The target was placed inside a quartz tube reactor heated to 700 °C. Pulsed laser ablation was conducted using a Nd:YAG laser (1064/532 nm, 10 Hz, 8 ns, 60 mJ per pulse) for 20 min. The generated soot was flushed back downstream by flowing argon gas and was collected on a quartz substrate, which was placed on a finger outside the oven. The gas flow rate was set to 200 cm^3 min^{-1} at atmospheric pressure. The inorganic fullerene-like particles were suspended by sonication in ethanol and then spread on lacy or quantifoil grids.

Experimental tilt-angle series of MoS_2 nanoparticles were acquired in a FEI Titan 80-300 transmission electron microscope equipped with a double-hexapole aberration corrector[14] for the objective lens. NCSI conditions were adjusted to achieve optimum phase contrast at minimized delocalization[17] at an accelerating voltage of 80 kV. Higher order aberrations were controlled by prealignment of the microscope by the aid of Zemlin tableaus.[25] High-resolution images were recorded at 3° intervals over a tilt range of $\pm 60°$ in manual operation in order to ensure accurate focusing with a tolerance of less than ± 5 nm. Image alignment was done by cross correlation of successive images in the tilt angle series followed by manual fine-tuning. 3D reconstruction and visualization were done in the same way as for the simulated images.

Figures 1 and 2 summarize the results of the simulation study. Figure 1a shows the atomic model of a regular double-shell nanooctahedron. In order to constrain the calculation time of the numerical image calculation, a small stoichiometric octahedron consisting of 320 stoichiometric units of MoS_2 in total was selected. The simulated electron microscopy images in Figure 1b were calculated for the optimum phase contrast conditions at the NCSI setting for 80 kV. In these single-projection images, a high-projected density of atoms corresponds to bright image dots relative to the mean intensity. In particular the sulfur atoms at the edges of the projected structures are well reproduced, albeit not fully resolved. The simulated images validate that the NCSI conditions produce single tilt-angle images which are a close approximate with the projected potential.

Figure 2 shows the tomographic reconstruction of a series of simulated images for a single-axis tilt of $\pm 60°$ symmetrically around the $\langle -516 \rangle$ orientation in Figure 1. Figure

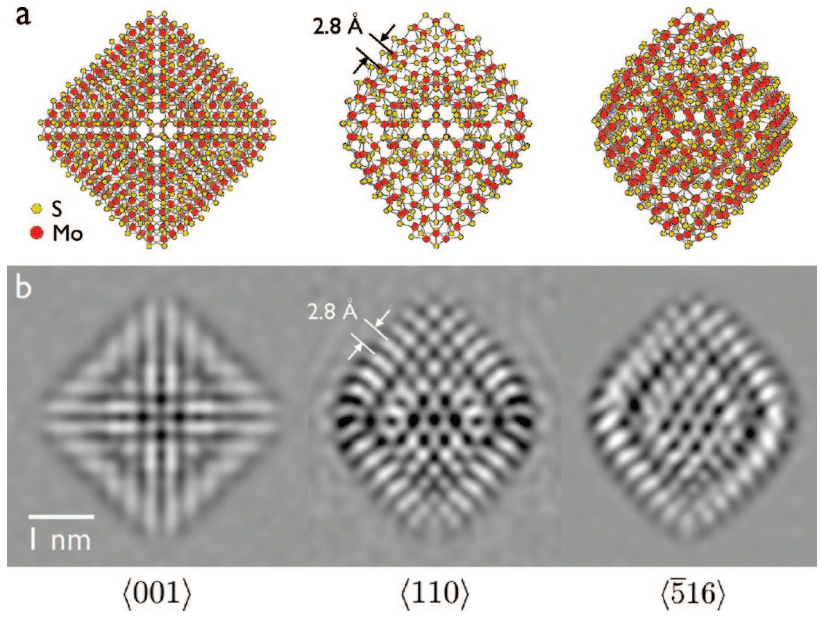

Figure 1. Model structure of a double-shell MoS_2 nanooctahedron. The model was calculated by a quantumn mechanical approach[12,13] and is viewed along various directions. (a) Atomic structure with 64 and 256 stoichiometric MoS_2 units in the inner and outer shells, respectively. (b) High-resolution TEM images simulated for optimized phase contrast at negative spherical aberration in an aberration-corrected microscope at 80 kV accelerating voltage. Bright contrast corresponds with projected atom positions.

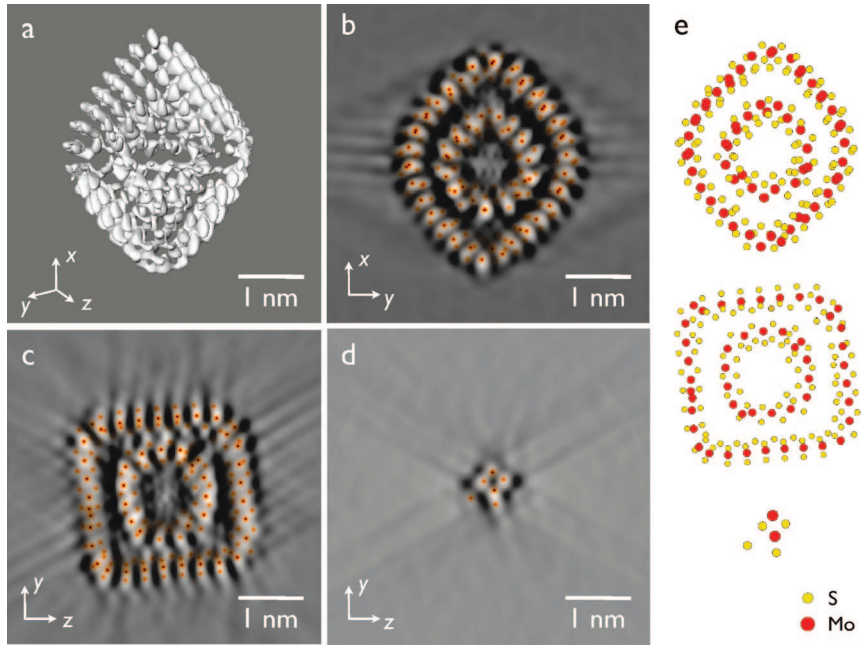

Figure 2. Single axis tomographic reconstruction from a tilt series of simulated images. A tilt range of 120° and an angular increment of 1° were chosen. By convention, *z* refers to the axis of transmission and *x* is parallel to the tilt axis in an orthogonal base system (*x*,*y*,*z*). (a) Isosurface visualization of the reconstructed tomogram of the closed cage structure model. (b−d) Slices taken in different planes and at different positions. Corresponding slices of the projected electrostatic potential of the model structure are superimposed in a red temperature scale. Strong dots represent Mo atoms; the weaker dots correspond to S atoms. (b) Tomogram slice in the *xy* plane through the center of the octahedron, corresponding to a slice in the ⟨−516⟩ orientation in Figure 1. (c) Central tomogram slice in the *yz* plane. (d) Tomogram slice in the *yz* plane through the apex of the structure showing the square defect in the seaming of the triangular faces. (e) The corresponding structure model slices.

2a displays an isosurface model of the reconstructed 3D volume. The shell structure and the hexagonal coordination of the molybdenum skeleton are retained. The resolution in the tomogram is theoretically limited by the number of images and the incomplete range of tilts (120°). The Crowther relation[24] states that the sampling in the tilt space limits the resolution of the tomographic reconstruction along the tilt axis theoretically to about 1 Å. The resolution orthogonal to the tilt axis is worse by an the elongation factor[6] of 1.5 due to the tilt range not spanning 180°. However in this case, the information limit of the microscope is about 2 Å and is therefore the limiting factor for the

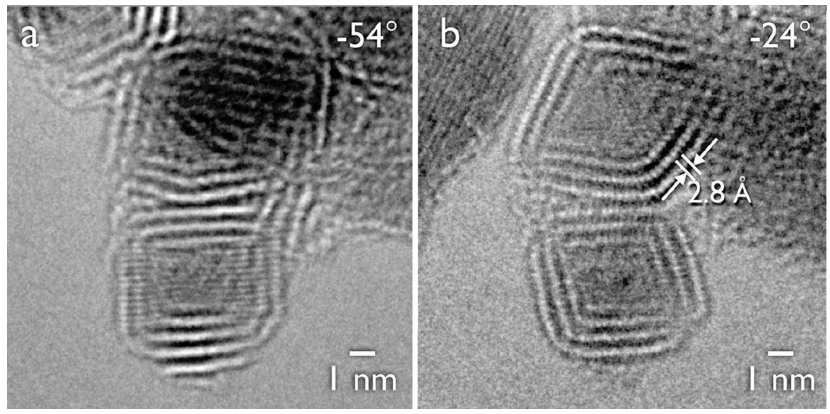

Figure 3. Experimental high-resolution TEM bright-field images. The images were taken close to the optimum phase contrast settings at negative spherical aberration at 80 kV accelerating voltage. Both images are taken from a tilt series with a tilt range of 120° in increments of 3°. The tilt axis is parallel to the vertical direction in these images. (a) Two nanooctahedra, adjoined on one of their faces and viewed along a direction of low symmetry. (b) The same octahedra viewed along a direction of high symmetry. Bright dots correspond to Mo positions with a projected distance of 2.8 Å.

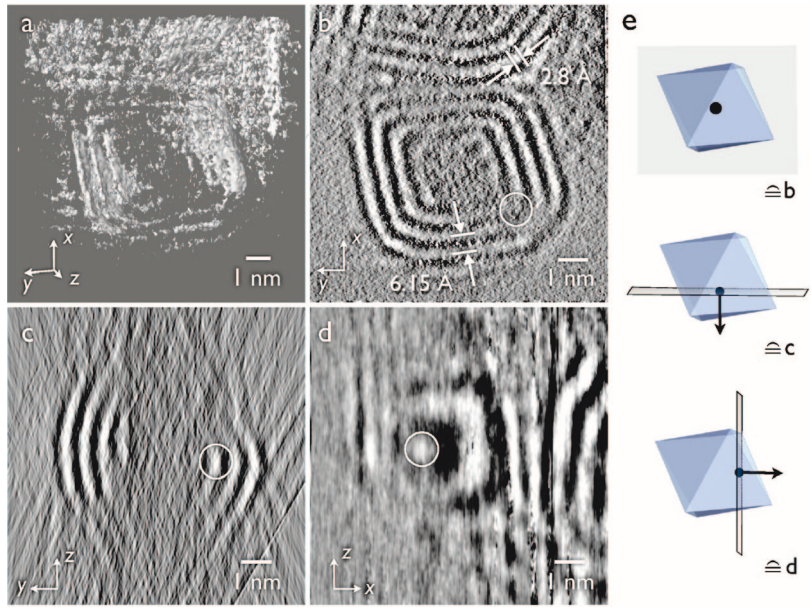

Figure 4. Experimental tomogram reconstructed from a single-axis tilt series of bright-field images. The images were taken over a tilt range of 63° in increments of 3°. *z* refers to the axis of transmission and *x* is parallel to the tilt axis in an orthogonal base system (*x*,*y*,*z*). (a) Isosurface representation showing the nested shell structure. (b−d) Tomogram slices in three orthogonal cut planes through the tip of the second shell (circular marker) of the lower octahedron. (e) Schematic drawings showing the orientation and position of the slice planes corresponding to (b−d). In all the slices the nested structure and the shell separation of 6.15 Å are clearly resolved. In the *xz* slice in (c) the square coordination of the triangular MoS_2 faces is observed for the third and fourth shell. In the upper part of the *xy* slice of the tomogram, the resolution of the projected distance between Mo units of ∼2.8 Å is retained.

resolution. Hence, the 2.41 Å separation between Mo and S is poorly resolved in contrast to the 3.16 Å separation between the Mo atoms.

Panels b−d of Figure 2 show slices from the tomogram and a superposition with accordingly projected potential slices taken from the model structure. It becomes evident that a projected potential map can be extracted directly from the tomogram. Regions of high tomogram intensity correspond with a high strength of the projected electrostatic potential. Thus the tomogram can be interpreted directly in terms of the atomic structure; it is not just showing lattice interference fringes. The tomogram, e.g., reconstitutes the coordination of Mo around the basal plane and the nonmirror symmetry in the seaming of three triangular MoS_2 faces. Another important feature exposed is the square defect at the apexes in the model structure (Figure 2d). The corresponding structure model slices are presented in Figure 2e for comparison. The tomographic reconstruction, based on images taken under NCSI conditions at 80 kV, is therefore capable of recovering essential information on the scale of better than 3 Å in all three dimensions.

Figure 3 shows two experimental images of two MoS_2 nanooctahedra taken from a single-axis tilt series with a tilt range of 120° in steps of 3°. The images were taken as close as possible to the optimum NCSI conditions at 80 kV. The multishell nanooctahedra, which are adjoined on one of their

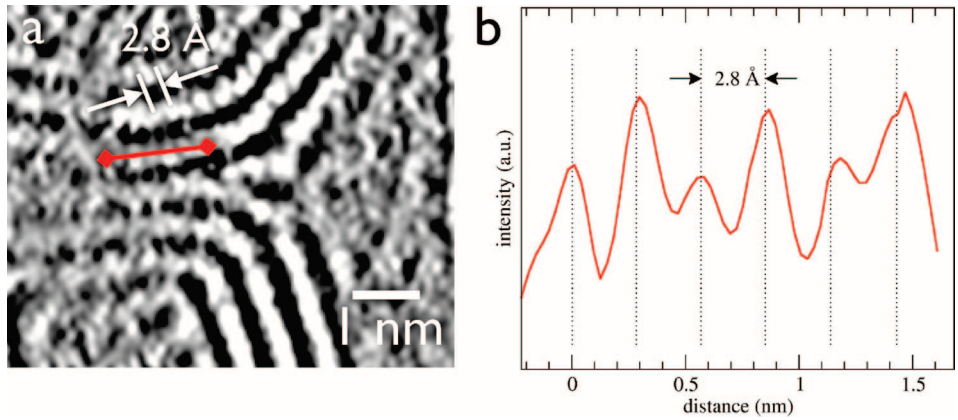

Figure 5. Spatial resolution in the *xy* plane of the experimental reconstruction. (a) Magnified region from the *xy* slice in Figure 4b. The bright dots in the shells correlate with the positions of Mo units. The line profile plotted in (b) shows the spacing between the dots in the tomogram. It corresponds with the projected distance between Mo units of ~2.8 Å, demonstrating a resolution better than this spacing.

triangular faces, are viewed along a direction of low symmetry in Figure 3a. Here, the close projected distance of atoms obstructs the image detail in one direction. Viewed along the high symmetry direction in Figure 3b, the Mo skeleton of the nanooctahedra is resolved. Dots with a spacing of 2.8 Å are well separated, corresponding to the projected distance of Mo atoms in the hexagonal Mo base lattice (see also Figure 1).

The tomogram in Figure 4 was reconstructed from a subset of 22 experimental images of the nanooctahedra in Figure 3, where the nanooctahedra are not overshadowed by neighboring structures. The nested shells with their smallest separation of 6.15 Å are reproduced in all of the slices, demonstrating the subnanometer resolution in the tomogram. In particular, the internal structure of the lower octahedron is unveiled. The hollow structure of the nanoparticles becomes obvious from the slice in Figure 4b. Another example for an internal sructure detail uncovered is a vertex of the second shell that is marked by a circle in panels b−d of Figure 4. Details of the atomic coordination at the vertex are still hidden in this tomographic reconstruction, since the missing wedge of 117° reduces the information available in the direction of transmission, *z*. The elongation factor[6] estimating the loss of spatial resolution for the *z* direction is calculated to about 3.1 for the present range of missing viewing angles, meaning that the resolution in the *z* direction is no more than the shell separation. The shell separation is less clearly resolved in the *z* direction than in the *x* and *y* direction for the same reason (see Figure 4). However, the resolution of 2.8 Å obtained for the projected Mo distances in the *xy* plane (see Figure 5) agrees with the predicted resolution better than 3 Å. The overall resolution in the experiment tomogram achieved so far is therefore about $0.3 \times 0.6 \times 0.6\ \text{nm}^3 = 0.11\ \text{nm}^3$, an improvement of nearly 1 order of magnitude compared to state of the art electron tomography schemes in the physical sciences. A wider tilt angle range and smaller increments will substantially improve the 3D resolution, as well as more sophisticated image acquisition and tomographic reconstruction schemes that have to be adapted to the requirements of atomic resolution.

In conclusion, we have demonstrated that 3D atomic resolution is feasible for fullerene-like structures through low-voltage aberration-corrected bright-field electron tomography. A first application clearly shows subnanometer spatial resolution of about 0.11 nm^3 on MoS_2 nanooctahedra.

Acknowledgment. R.T. holds the Drake Family Chair in Nanotechnology and is the director of the Helen and Martin Kimmel Center for Nanoscale Science. He acknowledges the support of the Harold Perlman Foundation. K.U. and L.H. wish to thank the German Science Foundation (DFG) for the financial support for subångström microscopy instrumentation at the Ernst Ruska-Centre.

Supporting Information Available: Videos showing slices from different planes. This material is available free of charge via the Internet at http://pubs.acs.org.

References

(1) Frank, J., *Electron Tomography: Three-dimensional imaging with the transmission electron microscope*; Plenum Press: New York, 1992.
(2) Baumeister, W.; Grimm, R.; Walz, J. *Trends Cell Biol.* **1999**, *9*, 81.
(3) Koster, A. J.; Ziese, U.; Verkleij, A. J.; Janssen, A. H.; de Jong, K. P. *J. Phys. Chem. B* **2000**, *104*, 9368.
(4) Koster, A. J.; Grimm, R.; Typke, D.; Hegerl, r.; Stoschek, A.; Walz, J.; Baumeister, W. *J. Struct. Biol.* **1997**, *120*, 276.
(5) McEwen, B. F.; Marko, M. *J. Histochem. Cytochem.* **2001**, *49*, 553.
(6) Midgley, P. A.; Weyland, M. *Ultramicroscopy* **2003**, *96*, 413.
(7) Kübel, C.; Voigt, A.; Schoenmakers, R.; Otten, M.; Su, D.; Lee, T.-C.; Carlsson, A.; Bradley, J. *Microsc. Microanal.* **2005**, *11*, 378.
(8) Möbus, G.; Inkson, B. J. *Appl. Phys. Lett.* **2001**, *79*, 1369.
(9) Tenne, R. *Nat. Nanotechnol.* **2006**, *1*, 103.
(10) Tenne, R.; Margulis, L.; Genut, M.; Hodes, G. *Nature* **1992**, *360*, 444.
(11) Tenne, R. *Adv. Mater.* **1995**, *7*, 965–989.
(12) Bar-Sadan, M.; Enyashin, A. N.; Gemming, S.; Popovitz-Biro, R.; Hong, S. Y.; Prior; Yehiam; Tenne, R.; Seifert, G. *J. Phys. Chem. B* **2006**, *110*, 25399.
(13) Enyashin, A. N.; Gemming, S.; Bar-Sadan, M.; Popovitz-Biro, R.; Hong, S. Y.; Prior, Y.; Tenne, R.; Seifert, G. *Angew. Chem., Int. Ed.* **2007**, *46*, 623.
(14) Haider, M.; Uhlemann, S.; Schwan, E.; Rose, H.; Kabius, B.; Urban, K. *Nature* **1998**, *392*, 768.
(15) Lentzen, M.; Jahen, B.; Jia, C. L.; Thust, A.; Tillman, K.; Urban, K. *Ultramicroscopy* **2002**, *92*, 233.
(16) Jia, C. L.; Lentzen, M.; Urban, K. *Science* **2003**, *299*, 870.
(17) Lentzen, M. *Microsc. Microanal.* **2006**, *12*, 191.
(18) Elstner, M.; Frauenheim, T.; McKelvey, J.; Seifert, G. *J. Phys. Chem. A* **2007**, *111*, 5607.
(19) Stadelmann, P. A. *Ultramicroscopy* **1987**, *21*, 131.

(20) IMOD homepage:http://bio3d.colorado.edu/imod/.
(21) Kremer, J. R.; Mastronarde, D. N.; McIntosh, J. R. *J. Struct. Biol.* **1996**, *116*, 71.
(22) Mastronarde, D. N. *J. Struct. Biol.* **1997**, *120*, 343.
(23) AMIRA homepage:http://www.tgs.com/products/amira.asp.
(24) Crowther, R. A.; Derosier, D. J.; Klug, A. *Proc. R. Soc. London, Ser. A* **1970**, *317*, 319.
(25) Uhlemann, S.; Haider, M. *Ultramicroscopy* **1998**, *72*, 109.

NL073149I